

Bragg reflection waveguide as a source of wavelength-multiplexed polarization-entangled photon pairs

Jiří Svozilík,^{1,2} Martin Hendrych,¹ and Juan P. Torres^{1,3}

¹*ICFO-Institut de Ciències Fòniques, UPC, Mediterranean Technology Park, 08860 Castelldefels (Barcelona), Spain*

²*Palacký University, RCPTM, Joint Laboratory of Optics, 17.listopadu 12, 771 46 Olomouc, Czech Republic*

³*Department of Signal Theory and Communications, Universitat Politècnica de Catalunya, Castelldefels, 08860 Barcelona, Spain*

jiri.svozilik@icfo.es

Abstract: We put forward a new highly efficient source of paired photons entangled in polarization with an ultra-large bandwidth. The photons are generated by means of a conveniently designed spontaneous parametric down-conversion process in a semiconductor type-II Bragg reflection waveguide. The proposed scheme aims at being a key element of an integrated source of polarization-entangled photon pairs highly suitable for its use in a multi-user quantum-key-distribution system.

© 2024 Optical Society of America

OCIS codes: (190.4410) Nonlinear optics, parametric processes; (270.0270) Quantum optics.

References and links

1. A. Serafini, S. Mancini, and S. Bose, “Distributed quantum computation via optical fibers,” *Phys. Rev. Lett.* **96**, 010503 (2006).
2. J. I. Cirac, A. K. Ekert, S. F. Huelga, and C. Macchiavello, “Distributed quantum computation over noisy channels,” *Phys. Rev. A* **59**, 4249–4254 (1999).
3. G. Ribordy, J. Brendel, J. Gautier, N. Gisin, and H. Zbinden, “Long-distance entanglement-based quantum key distribution,” *Phys. Rev. A* **63**, 012309 (2000).
4. A. K. Ekert, “Quantum cryptography based on Bells theorem,” *Phys. Rev. Lett.* **67**, 661–663 (1991).
5. M. Hillery, V. Bužek, and A. Berthiaume, “Quantum secret sharing,” *Phys. Rev. A* **59**, 1829–1834 (1999).
6. C. H. Bennett, G. Brassard, C. Crepeau, R. Jozsa, A. Peres, and W. K. Wootters, “Teleporting an unknown quantum state via dual classical and Einstein-Podolsky-Rosen channels,” *Phys. Rev. Lett.* **70**, 1895–1899 (1993).
7. T. S. Humble, and W. P. Grice, “Spectral effects in quantum teleportation,” *Phys. Rev. A* **75**, 022307 (2007).
8. H. Hubel, M. R. Vanner, T. Lederer, B. Blauensteiner, T. Lorunser, A. Poppe, and A. Zeilinger, “High-fidelity transmission of polarization encoded qubits from an entangled source over 100 km of fiber,” *Opt. Express* **15**, 7853–7862 (2007).
9. T. E. Chapuran, P. Toliver, N. A. Peters, J. Jackel, M. S. Goodman, R. J. Runser, S. R. McNown, N. Dallmann, R. J. Hughes, K. P. McCabe, J. E. Nordholt, C. G. Peterson, K. T. Tyagi, L. Mercer, and H. Dardy, “Optical networking for quantum key distribution and quantum communications,” *New J. Phys.* **11**, 105001 (2009).
10. A. L. Migdall, D. Branning, and S. Castelletto, “Tailoring single-photon and multiphoton probabilities of a single-photon on-demand source,” *Phys. Rev. A* **66**, 053805 (2002).
11. J. H. Shapiro, and F. N. Wong, “On-demand single-photon generation using a modular array of parametric down-converters with electro-optic polarization controls,” *Opt. Lett.* **32**, 2698–2700 (2007).
12. A. Fedrizzi, T. Herbst, A. Poppe, T. Jennewein, and A. Zeilinger, “A wavelength-tunable fiber-coupled source of narrowband entangled photons,” *Opt. Express* **15**, 15377–15386 (2007).
13. H. C. Lim, A. Yoshizawa, H. Tsuchida, and K. Kikuchi, “Wavelength-multiplexed distribution of highly entangled photon-pairs over optical fiber,” *Opt. Express* **26**, 22099–22104 (2008).

14. P. Abolghasem, J. Han, B. J. Bijlani, A. Arjmand, and A. S. Helmy, "Continuous-wave second harmonic generation in Bragg reflection waveguides," *Opt. Lett.* **34**, 9460–9467 (2009).
15. K. Thyagarajan, R. Das, O. Alibart, M. Micheli, D. B. Ostrowsky, and S. Tanzilli, "Increased pump acceptance bandwidth in spontaneous parametric downconversion process using Bragg reflection waveguides," *Opt. Express* **16**, 3577–3582 (2008).
16. D. Kang and A. S. Helmy, "Generation of polarization entangled photons using concurrent type-I and type-0 processes in AlGaAs ridge waveguides," *Opt. Lett.* **37**, 1481–1483 (2012).
17. I. Shoji, T. Kondo, A. Kitamoto, M. Shirane, R. Ito, "Absolute scale of second-order nonlinear-optical coefficients," *J. Opt. Soc. Am. B* **14**, 2268–2294 (1997).
18. B. J. Bijlani, and A. S. Helmy, "Bragg reflection waveguide diode lasers," *Opt. Lett.* **34**, 3734–3736 (2009).
19. R. Horn, P. Abolghasem, B. J. Bijlani, D. Kang, A. S. Helmy, and G. Weihs, "Monolithic source of photon pairs," *Phys. Rev. Lett.* **108**, 153605 (2012).
20. A. S. Helmy, B. Bijlani, and P. Abolghasem, "Phase matching in monolithic Bragg reflection waveguides," *Opt. Lett.* **32**, 2399–2401 (2007).
21. J. P. Torres, K. Banaszek, and I. A. Walmsley, "Engineering nonlinear optic sources of photonic entanglement," *Prog. Optics* **56**, 227–331 (2011).
22. S. V. Zhukovsky, L. G. Helt, D. Kang, P. Abolghasem, A. S. Helmy, and J. E. Sipe, "Generation of maximally-polarization-entangled photons on a chip," *Phys. Rev. A* **85**, 013838 (2012).
23. J. P. Torres, M. Hendrych, and A. Valencia, "Angular dispersion: an enabling tool in nonlinear and quantum optics," *Adv. Opt. Photon.* **2**, 319–369 (2010).
24. J. Jin, *The finite element method in electromagnetics, 2nd Edition*, (Wiley-IEEE Press, 2002).
25. S. Gehrsitz, F. K. Reinhart, C. Gourgon, N. Herres, A. Vonlanthan, and H. Sigg, "The refractive index of Al(x)Ga(1-x)As below the band gap: accurate determination and empirical modeling," *J. Appl. Phys.* **87**, 7825–7837 (2000).
26. A. Ling, A. Lamas-Linares, and C. Kurtstiefer, "Absolute emission rates of spontaneous parametric down-conversion into single transverse Gaussian modes," *Phys. Rev. A* **77**, 043834 (2008).
27. S. Hill, and W. K. Wootters, "Entanglement of a pair of quantum bits," *Phys. Rev. Lett.* **78**, 5022–5025 (1997).
28. K. Wootters, "Entanglement of formation of an arbitrary state of two qubits," *Phys. Rev. Lett.* **80**, 2245–2248 (1998).
29. T. Yu, and J. H. Eberly, "Quantum open system theory: bipartite aspects," *Phys. Rev. Lett.* **97**, 140403 (2006).
30. Y. Kim, and W. P. Grice, "Reliability of the beam-splitterbased Bell-state measurement," *Phys. Rev. A* **68**, 062305 (2003).
31. P. P. Rohde, and T. C. Ralph, "Frequency and temporal effects in linear optical quantum computing," *Phys. Rev. A* **71**, 032320 (2005).
32. W. Drexler, "Ultra-high-resolution optical coherence tomography," *J. Biomedical Opt.* **9**, 47–74 (2004).

1. Introduction

Many quantum computing applications [1, 2] and quantum communication protocols [3–5], such as quantum teleportation [6, 7], are based on the sharing of entangled two-photon states between two distant receiving stations. The paired photons can be distributed through free space transmission channels, or alternatively, through single-mode fiber optical links. Indeed, fiber optical links are the most practical way to share entanglement between a large number of users.

The polarization degree of freedom is the most widely used resource to generate entanglement between two distant parties. Polarization-entangled photons can be generated by means of spontaneous parametric down-conversion (SPDC), a nonlinear optical process in which two lower-frequency photons (signal and idler) are generated when a strong pump interacts with the atoms of a nonlinear material. Subsequently to the generation, each photon constituting a pair can propagate through a different single-mode fiber, with the initial degree of entanglement between the photons being preserved over long distances [8].

One application that is attracting a lot of interest due its potential key role in the newly emerging quantum communication networks is the multi-user quantum key distribution (QKD) [9]. In order to implement a multi-user QKD network, various frequency channels can expediently be employed for transmitting individual entangled pairs. In this way, one can re-route on demand specific channels between users located in different sites of the optical network. Similar schemes, considering the emission of photon pairs in different spectral and spatial modes, have been presented in [10, 11] for an on-demand single-photon source based on a single crystal.

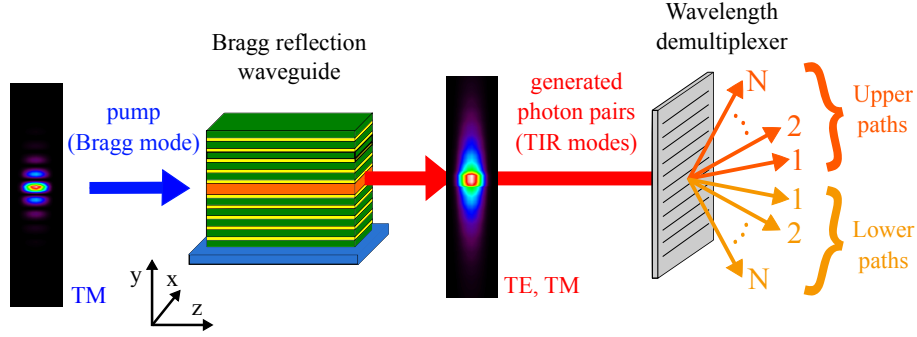


Fig. 1. General scheme for the generation of polarization-entangled photon pairs in various frequency channels by making use of the Bragg reflection waveguide. In this scheme, a dichroic mirror or a grating can be used as the wavelength demultiplexer.

To prepare polarization-entangled paired photons in many frequency channels at the same time, one needs to engineer an SPDC process with an ultra-broad spectrum. Usually type-I or type-0 configurations are preferred. With the type-II phase-matching, the two down-converted photons have different polarizations and consequently different group velocities, which reduces dramatically their bandwidth. For instance, the FWHM bandwidth of an SPDC process in a type-II periodically-poled (PP) KTP crystal at 810 nm is given by $\Delta\lambda(\text{nm}) = 5.52/L(\text{mm})$, where L is the length of the crystal [12]. For $L = 1$ mm, the bandwidth is $\Delta\lambda \sim 5.5$ nm. On the other hand, in a type-0 PPLN configuration with the same crystal length $L = 1$ mm, Lim et al. [13] achieved an approximate tenfold increase of the bandwidth $\Delta\lambda \sim 50$ nm. Even though one can always reduce the length of the nonlinear crystal in a type-II configuration to achieve an increase of the bandwidth, this results in a reduction of the spectral brightness of the source.

Alternatively to short bulk crystals, Bragg reflection waveguides (BRWs) based on III-V ternary semiconductor alloys ($\text{Al}_x\text{Ga}_{1-x}\text{As}$) offer the possibility to generate polarization-entangled photons with an ultra-large bandwidth. The most striking feature of the use of BRW as a photon source is the capability of controlling the dispersive properties of all interacting waves in the SPDC process, which in turn allows the tailoring of the bandwidth of the down-converted photons: from narrowband (1 – 2 nm) to ultra-broadband (hundreds of nm) [14–16], considering both type-I and type-II configurations. Therefore, one can design a type-II SPDC process in BRWs with a bandwidth typical for type-I or type-0 processes.

The utilization of Bragg reflection waveguide (BRW) has further advantages over other conventional SPDC sources due to the large nonlinear coefficient of semiconductors ($d_{\text{eff}}^{\text{GaAs}} \sim 119$ pm/V) [17], broad transparency window (0.9 - 17 μm) and mature fabrication technologies that can be used for integration of the source of entangled photons with a light source and other optical elements. Additionally, a laser based on BRWs has already been demonstrated [18], opening a door for the integration in a single chip of the pump light source together with the BRW, where the down-converted photons are generated [19].

$\text{Al}_x\text{Ga}_{1-x}\text{As}$ is an optically isotropic semiconductor, precluding birefringent phase matching. However, the modal phase-matching of the interacting waves (pump, signal and idler) can be achieved by letting each wave propagate in a different type of mode supported by the waveguide. For instance, the phase-matching can be successfully achieved if the pump propagates in the waveguide in a Bragg mode, whereas the signal and idler photons propagate in total-internal-reflection (TIR) modes [20].

2. Description of the quantum state of the down-converted photons

In order to investigate the potential of the proposed design for generating wavelength-multiplexed polarization-entangled photon pairs over many frequency channels, let us examine the biphoton generation in a collinear type-II phase-matching scheme in the Bragg reflection waveguide (see Fig. 1). A continuous-wave TM-polarized pump beam with frequency ω_p illuminates the waveguide and mediates the generation of a pair of photons with mutually orthogonal polarizations (signal: TE polarization; idler: TM polarization). The frequencies of the signal and idler photons are $\omega_s = \omega_0 + \Omega$ and $\omega_i = \omega_0 - \Omega$, respectively, where ω_0 is the degenerate central angular frequency of both photons, and Ω is the angular frequency deviation from the central frequency. The signal photon (TE) propagates as a TIR mode of the waveguide with spatial shape $U_s(x, y, \omega_s)$ and propagation constant $\beta_s(\omega_s)$. The idler photon (TM), also a TIR mode, has a spatial shape $U_i(x, y, \omega_i)$ and propagation constant $\beta_i(\omega_i)$. The pump beam is a Bragg mode of the waveguide with spatial shape $U_p(x, y, \omega_p)$ and propagation constant $\beta_p(\omega_p)$.

At the output face of the nonlinear waveguide, the quantum state of the biphoton can be written as [21]

$$|\Psi_1\rangle = |\text{vac}\rangle_s |\text{vac}\rangle_i + \sigma L F_p^{1/2} \int d\Omega \Phi(\Omega) |\text{TE}, \omega_0 + \Omega\rangle_s |\text{TM}, \omega_0 - \Omega\rangle_i, \quad (1)$$

where the nonlinear coefficient σ is defined

$$\sigma = \left[\frac{\hbar \omega_0^2 \omega_p [\chi^{(2)}]^2 \Gamma^2}{16\pi \epsilon_0 c^3 n_s(\omega_0) n_i(\omega_0) n_p(\omega_p)} \right]^{1/2}. \quad (2)$$

F_p is the flux rate of pump photons, $\Gamma = \int d\mathbf{r}_\perp U_p(\mathbf{r}_\perp) U_s^*(\mathbf{r}_\perp) U_i^*(\mathbf{r}_\perp)$ is the overlap integral of the spatial modes of all interacting waves in the transverse plane, and $n_{p,s,i}$ are their refractive indices. The joint spectral amplitude $\Phi(\Omega)$ has the form

$$\Phi(\Omega) = \text{sinc} [\Delta_k(\Omega)L/2] \exp \{i s_k(\Omega)L/2\}. \quad (3)$$

The ket $|\text{TE}, \omega_0 + \Omega\rangle_s$ ($|\text{TM}, \omega_0 - \Omega\rangle_i$) designates a signal (idler) photon that propagates with polarization TE (TM) in a mode of the waveguide with the spatial shape U_s (U_i) and frequency $\omega_0 + \Omega$ ($\omega_0 - \Omega$). The phase-mismatch function reads $\Delta_k(\Omega) = \beta_p - \beta_s(\Omega) - \beta_i(-\Omega)$, and $s_k(\Omega) = \beta_p + \beta_s(\Omega) + \beta_i(-\Omega)$. The function $|\Phi(\Omega)|^2$ is proportional to the probability of detection of a photon with polarization TE and frequency $\omega_0 + \Omega$ in coincidence with a photon with TM polarization and frequency $\omega_0 - \Omega$.

After the waveguide, a wavelength demultiplexer is used to separate all n frequency channels into coupled fibers leading to the users of the network. The bandwidth of each channel is $\Delta\omega$ and their central frequencies are $\omega_{U,L}^n = \omega_0 \pm n\Delta$, where Δ is the inter-channel frequency spacing and the letter U(L) indicates the upper (lower) path (see Fig. 1). After the demultiplexer, the quantum state of the down-converted photons can be written as

$$\begin{aligned} |\Psi_2\rangle &= |\text{vac}\rangle_s |\text{vac}\rangle_i \\ &+ 1/\sqrt{2} \sigma L F_p^{1/2} \int_{B_n} d\Omega \{ \Phi(\Omega) |\text{TE}, \omega_0 + \Omega\rangle_U |\text{TM}, \omega_0 - \Omega\rangle_L \\ &+ \Phi(-\Omega) |\text{TM}, \omega_0 + \Omega\rangle_U |\text{TE}, \omega_0 - \Omega\rangle_L \}, \end{aligned} \quad (4)$$

where \int_{B_n} designates the frequency bandwidth from $\omega_{U,L}^n - \Delta\omega/2$ to $\omega_{U,L}^n + \Delta\omega/2$ coupled into every single fiber. Since we are interested in generating polarization-entangled paired photons coupled into single-mode fibers, the signal and idler photons in the upper and lower paths

Table 1. (a) Parameters of the structure: t_c - core thickness; $t_{1,2}$ - thicknesses of the alternating layers of the Bragg reflector; x_c - aluminium concentration in the core; $x_{1,2}$ - aluminium concentrations in the reflector's layers; n_c - the refractive index in the core; $n_{1,2}$ - refractive indices in the reflector's layers; $\partial\beta_{s(i)}/\partial\Omega$ -the inverse group velocity of the signal (idler) photon. The structure is optimized for the collinear type-II SPDC. (b) Profile of the refractive index along the y -axis of the BRW.

Parameter	Value
t_c (nm)	370
t_1 (nm)	127
t_2 (nm)	309
$n_c(x_c = 0.7)$	3.177
(a) $n_1(x_1 = 0.4)$	3.655
$n_2(x_2 = 0.9)$	3.064
Ridge width (nm)	1770
$\partial\beta_s/\partial\Omega$ (ns/m)	10.55
$\partial\beta_i/\partial\Omega$ (ns/m)	10.56
Waveguide length (mm)	1

are projected into the fundamental mode (U_0) of the fiber. The coupling efficiency between the signal and idler modes, and the fundamental mode of the single-mode fiber are given by $\Gamma_s = |\int dx dy U_s(x, y, \omega_s) U_0^*(x, y, \omega_0)|^2$ and $\Gamma_i = |\int dx dy U_i(x, y, \omega_i) U_0^*(x, y, \omega_0)|^2$. They yield a value of $\Gamma_s = \Gamma_i \approx 0.88$ in the whole bandwidth of interest, showing a minimal frequency dependence. All the modes are normalized so that $\int dx dy |U_j(x, y, \omega)|^2 = 1$ for $j = s, i, 0$.

Neglecting the vacuum contribution in the final quantum state, normalizing and tracing out the frequency degree of freedom, the two-photon state can be represented by the following density matrix, where we use the conventional ordering of rows and columns as $\{|TE\rangle_U |TE\rangle_L, |TE\rangle_U |TM\rangle_L, |TM\rangle_U |TE\rangle_L, |TM\rangle_U |TM\rangle_L\}$:

$$\rho_n = \begin{pmatrix} 0 & 0 & 0 & 0 \\ 0 & \alpha_n & \gamma_n & 0 \\ 0 & \gamma_n^* & \beta_n & 0 \\ 0 & 0 & 0 & 0 \end{pmatrix}, \quad (5)$$

where

$$\begin{aligned} \alpha_n &= 1/2 \int_{B_n} d\Omega |\Phi(\Omega)|^2, \\ \beta_n &= 1/2 \int_{B_n} d\Omega |\Phi(-\Omega)|^2, \\ \gamma_n &= 1/2 \int_{B_n} d\Omega \Phi(\Omega) \Phi^*(-\Omega), \end{aligned} \quad (6)$$

with $\text{Tr}[\rho_n] = \alpha_n + \beta_n = 1$.

3. Numerical results

In the waveguide structure considered, the pump wavelength is 775.1 nm. The frequency spacing between channels is $\Delta = 50$ GHz and the bandwidth of each channel is 50 GHz, which corresponds approximately to 0.4 nm at 1550 nm. The channel width and the spacing between

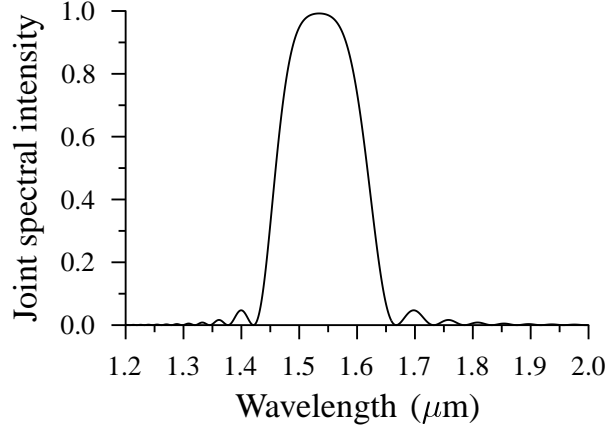


Fig. 2. Joint spectral intensity $\sim |\Phi(\lambda)|^2$ of the biphoton generated in the Bragg reflection waveguide for type-II phase-matching (TM \rightarrow TE + TM).

channels were chosen according to the typical values used in commercial WDM systems. Channel $n = 1$ corresponds to the wavelength 1549.6 nm in the upper path and to 1550.6 nm in the lower path.

In order to reach a high number of frequency channels, the BRW structure must be designed in such way, so as to permit the generation of signal-idler pairs with an ultra-broad spectrum in the type-II configuration. This is achieved when the group velocities of the TE and TM modes are equal [22,23], i.e., $|\frac{\partial \beta_s}{\partial \Omega} - \frac{\partial \beta_i}{\partial \Omega}| \rightarrow 0$. The modes of the structure and its propagation constants are obtained as a numerical solution of the Maxwell equations inside the waveguide using the finite element method [24]. The waveguide design has been optimized by a genetic algorithm according to the requirements. The final BRW design is composed of two Bragg reflectors, one placed above and one below the core. Each reflector contains 8 bi-layers. The Sellmeier equations for the refractive indices of the layers were taken from [25]. Table 1 summarizes the main parameters of the structure.

Inspection of Eq. (2) shows that the effective nonlinearity σ of the waveguide SPDC process depends on the effective area ($A_{\text{eff}} = 1/\Gamma^2$), which is related to the spatial overlap of the pump, signal and idler modes. For the structure considered, the effective area exhibits only minimal frequency dependence in the bandwidth of interest and it is equal to $A_{\text{eff}} = 35.3 \mu\text{m}^2$. Despite the fact that the large effective area will reduce the strength of the interaction, the high nonlinear coefficient still results in an efficiency that is a much higher than for other phase-matching platforms in waveguides or in bulk media. The total emission rate [26] can be expressed using Eq. (1) as $R = \sigma^2 L^2 \int d\Omega |\Phi(\Omega)|^2$. For our BRW, the emission rate is $R_{\text{BRW}} \approx 5.7 \times 10^7$ photons/s/mW. For comparison, for a typical PPLN waveguide (type-0) similar to the one used in [13], we obtain $R_{\text{PPLN}} \approx 3.3 \times 10^7$ photons/s/mW. The intensity of the joint spectral amplitude, given by Eq. (3), is displayed in Fig. 2. Even though we are considering a type-II configuration, the width (FWHM) of the spectrum is a staggering 160 nm.

The degree of entanglement in each spectral channel can be quantified by calculating the concurrence C_n of the biphoton [27,28]. The concurrence is equal to 0 for a separable state and to 1 for a maximally entangled state. For the density matrix of Eq. (5) we obtain [29]

$$C_n = 2|\gamma_n|, \quad (7)$$

so the degree of entanglement depends on the symmetry of the spectral amplitude $\Phi(\Omega)$, i.e.,

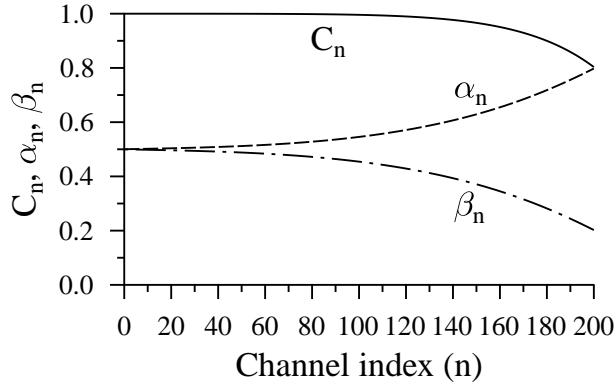


Fig. 3. Coefficients C_n (solid line), α_n (dashed line) and β_n (dotted-and-dashed line) as a function of the frequency channel.

if $\Phi(\Omega) = \Phi(-\Omega)$ the concurrence is maximum.

Figure 3 shows the values of α_n , β_n and C_n for the first 200 channels. $C_n > 0.9$ is reached for the first 179 channels. The decrease (increase) of the parameters β_n (α_n) reflects the fact that for frequency channels with a large detuning from the central frequency, one of the two polarization components of the polarization entangled state, $|\text{TE}\rangle_1|\text{TM}\rangle_2$ or $|\text{TM}\rangle_1|\text{TE}\rangle_2$, shows a greater amplitude probability. In this case, one of the two options predominates. Therefore, if the goal is to generate a quantum state of the form $|\Psi_2\rangle = 1/\sqrt{2} (|\text{TE}\rangle_1|\text{TM}\rangle_2 + |\text{TM}\rangle_1|\text{TE}\rangle_2)$ in a specific frequency channel with $\alpha_n, \beta_n \neq 1/2$, one can always modify the diagonal elements of the density matrix with a linear transformation optical system, keeping unaltered the degree of entanglement.

The number of frequency channels available depends on the concurrence required for the specific application. A good example is a linear optical gate relying on the interference of photons on a beam splitter [30, 31]. This would be especially important for the implementation of quantum teleportation, where the fidelity of the protocol depends strongly on the spectral indistinguishability between polarizations of the entangled state [7]. In Fig. 4 we plot the number of frequency channels available as a function of the minimum concurrence required. For instance, if we select only frequency channels with $C_n > 0.95$, we have at our disposal 162 channels, while for $C_n > 0.99$ this number is reduced to 121 channels.

In the implementation of the system considered here in a *real* fiber-optics network, the number of frequency channels available can be limited by several factors. For instance, it can be limited by the operational bandwidth of the demultiplexer (see Fig.1). This device should be designed to operate with the same broad spectral range of the photon pairs generated in the BRW waveguide.

When using a large number of channels, inspection of Fig. 2 shows that channels far apart from the central frequency will exhibit a lower brightness. In this case, spectral shapers or appropriately designed filters, should be used to flatten the emission spectrum, similarly to the case of broadband gain-flattened Erbium doped fiber amplifiers (EDFA). Notwithstanding, this might introduce some losses in the generation process, especially when considering a large number of channels, deteriorating the flux rate of the source. Interestingly, a similar problem appears in the context of optical coherence tomography (OCT), where large bandwidths are required to increase the imaging resolution. In OCT, spectral shapers are used to obtain an optimum (Gaussian-like) spectral shape [32].

Finally, we should mention that the generation of polarization-entangled photons with the

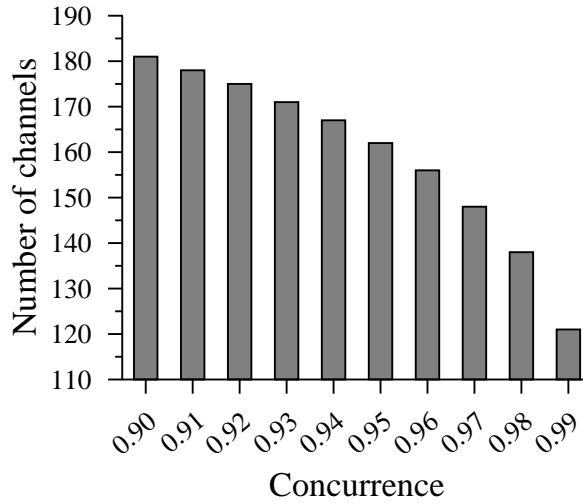


Fig. 4. Number of channels available as a function of the minimum value of the concurrence required.

large bandwidths considered here require a precise control the group velocities of the interacting waves, which in turn requires a precise control of the waveguide parameters: refractive index and layer widths. The effective number of available frequency channels in a specific application is inevitably linked to the degree of control of the fabrication process. Since both down-converted photons are propagating as TIR modes, they are more resistant to fabrication imperfections. For example, a change of about 10% in the aluminium concentration in the core will reduce the spectral bandwidth to 145 nm. Notwithstanding, it has to be stressed that the phase-matching condition for interacting waves is highly sensitive to any fabrication imperfection, therefore any small change of the structural parameters will lead to a shift of the central (phase-matched) wavelength.

4. Conclusion

In conclusion, we have presented a new type of highly efficient waveguide source for generating polarization-entangled photon pairs for its use in multi-frequency QKD networks. In spite of being a type-II SPDC source, the achieved bandwidth is even larger than the bandwidth usually obtained with type-I or type-0 sources. The key enabling factor that allows us to achieve high efficiency of the nonlinear process together with a bandwidth increase is the fact that we can use a longer nonlinear material in a type-II configuration, while at the same time keeping the broadband nature of the SPDC process through the appropriate design of the Bragg reflection waveguide structure.

Even though *conventional* sources based on the use of more common nonlinear materials, such as KTP or LiNbO₃, might also generate entangled pairs of photons with a large bandwidth, BRWs based on AlGaAs compounds offer two main advantages: an enhanced capability to tailor the general properties of the downconverted photons, and the possibility of integration of different elements (pump source, nonlinear waveguide and diverse optical elements) in a chip platform based on an already mature technology, which could pave the way for entanglement-based technologies in *out-of-the-lab scenarios*.

Acknowledgments

This work was supported by Project FIS2010-14831 and FET-Open 255914 (PHORBITECH). J. S. thanks the project FI-DGR 2011 of the Catalan Government. This work has also supported in part by projects COST OC 09026, CZ.1.05/2.1.00/03.0058 of the Ministry of Education, Youth and Sports of the Czech Republic and by projects PrF-2011-009 and PrF-2012-003 of Palacký University.